Field Modeling with Sampled Distances

Michael Freytag* Vadim Shapiro† Igor Tsukanov‡

Spatial Automation Laboratory
University of Wisconsin-Madison
1513 University Avenue
Madison, WI, 53706-1572, USA

Abstract

Traditional mesh-based approaches to the modeling and analysis of physical fields within geometric models require some form of topological reconstruction and conversion in the mesh generation process. Such manipulations tend to be tedious and error-prone manual processes that are not easily automated. We show that most field problems may be solved directly by using approximate distance fields computed from designed or sampled geometric data, thus avoiding many of the difficult reconstruction and meshing problems. With distances we can model fields that satisfy boundary conditions while approximating the governing differential equations to arbitrary precision. Because the method is based on sampling, it provides natural control for multi-resolution both in geometric detail of the domain and in accuracy of the computed physical field. We demonstrate the field modeling capability with several heat transfer applications, including a typical transient problem and a "scan and solve" approach to the simulation of a physical field in a real-world artifact.

1 Introduction

1.1 Field modeling with distances

Representation conversion of geometric data to a form compatible with the traditional mesh-based simulation pipeline requires a number of non-trivial automated and manual steps. The output of the pipeline is a physically meaningful, spatially and possibly temporally distributed quantity called a field. We thus refer to the entire simulation process as *field modeling*. Field simulation on CAD geometry, arguably the most common type of analysis, usually involves manual defeaturing to remove small features in order to produce domain meshes possessing elements of reasonable size. More complex analyses involving motion or deformation require manual domain meshing or the development of specialized software to produce suitable meshes. Field analysis on surface scan data captured from real-world objects requires manually-guided reconstruction of various types, healing, and simplification to produce a surface mesh capable of supporting domain meshing. Similar steps are required for isosurface meshes computed from volumetric data captured by such scanning technologies as CT, MRI and cryosectioning. The manual intervention required to produce domain meshes from such a variety of geometric data sources hinders automated preparation for field analysis. Further, it is widely accepted that today data preparation, and not the physical computations, dominate most field modeling problems both in terms of human effort and computer time.

We propose to replace the typical manual and error-prone conversions by an automated meshfree modeling method that relies on approximate distance fields to satisfy all boundary conditions as accurately as desired. The main idea is diagrammed in Figure 1. The approximate distance field may be defined and constructed by a variety of methods; in this paper, the approximate distance field is fit to samples of exact signed distance to the geometry.

The original idea of this meshfree method dates back to Kantorovich who proposed to represent a field that satisfies Dirichlet boundary conditions as the product of two functions: $u = \omega\Phi$, where $\omega = 0$ is an implicit representation of

*E-mail: freytag@sal-cnc.me.wisc.edu
†Corresponding author; E-mail: vshapiro@engr.wisc.edu
‡E-mail: tsukanov@engr.wisc.edu

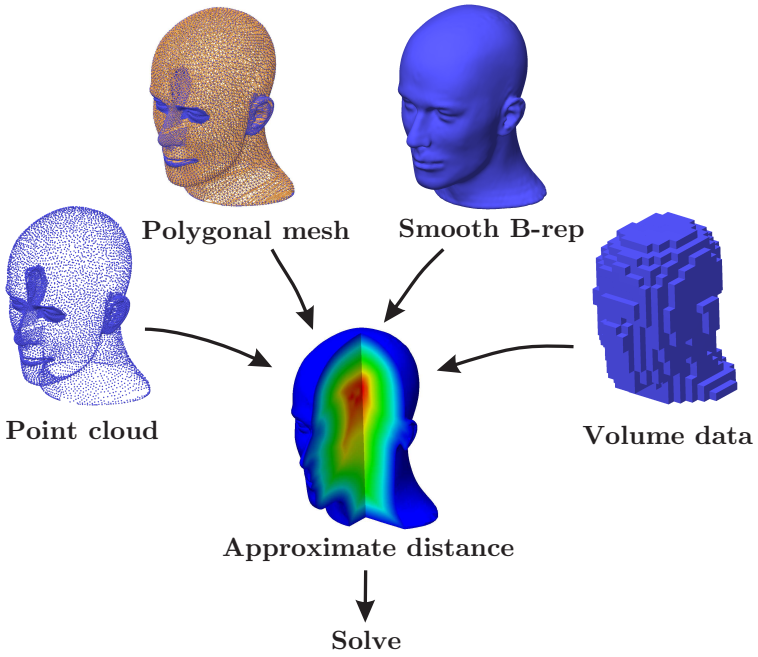

Figure 1: Figure depicts field modeling using approximate distance fields from surface points, polygonal surfaces, smooth B-rep, and volumetric data. The simplicity of the approach is in stark contrast to the multiple representation conversions required in traditional mesh-based analysis.

geometry with zero set corresponding to the geometry and non-vanishing gradient at all points of the zero set [9]. A key feature of this formulation is the ability to exactly satisfy the boundary conditions on the zero set of ω. Rvachev generalized Kantorovich's approach to include virtually all types of boundary value problems [20, 21]. Shapiro and Tsukanov showed that the method may be completely automated for a wide class of geometric and physical problems in a common meshfree environment[33, 32, 36]. Theoretical completeness of the method is shown in [22]. More recently, Höllig improved the numerical stability of this approach by approximating the function Φ by linear combinations of weighted extended B-splines (WEB-splines) [8, 7]. In this paper we show that Rvachev's approach to satisfy boundary conditions can be extended to modeling physical fields with approximate distance fields constructed through sampling. Our method can be viewed as a generalized finite element method that satisfies boundary conditions exactly[2]. Through sampling we extend the benefits of the meshfree method to a much larger class of problems, with multi-resolution, where previously automated solutions were not possible.

After briefly summarizing related work on approximate distance fields below, we discuss the details of our method, its treatment of different boundary conditions, and its application to field problems with different governing equations and boundary conditions. Sections 2 and 3 detail the formulation of the method in the context of homogeneous and non-homogeneous Dirichlet boundary conditions respectively. Section 4 extends the discussion to other types of boundary value problems and demonstrates the unique ability of the proposed method to control geometric and physical resolution. Section 5 describes two more challenging and interesting applications of the method to engineering problems. We close with a brief summary and discussion of the promising directions for future work.

1.2 Related Work on Distance Fields

Distance fields are scalar fields whose evaluation at any point returns the exact distance to the geometry. As suggested in Figure 1, distance fields can be computed from most geometric representations, including clouds of points, meshes, triangulations, boundaries, volumetric data, and other unambiguous representations. By definition, the exact distance field is differentiable and has unit gradient everywhere except the points that are equidistant from several points (e.g. points on medial axis). The zero set of the exact distance field corresponds to and implicitly defines the geometric set

of points.

In order to solve field modeling problems, we replace the exact distance fields with their approximations that are required to be differentiable to some order and possess non-vanishing gradient near their zero set [3]. In contrast to exact distance, approximate distance fields may introduce error between their zero set and the true geometric boundary, can possess gradient magnitudes different from 1, and may differ from the exact distance at any point in space. As shown by Rvachev and others, approximate distance fields, whose zero set coincides with the boundaries of geometric objects, can be constructed using R-functions while representing corners and edges exactly [20, 28, 32].

Many implicit geometric representations satisfy the properties of approximate distance fields [6, 4, 17]. Shapiro proposed algorithms for automatic construction of such implicit representations from both Constructive Solid Geometry and Boundary Representations of geometric objects [29, 30, 31]. Implicit representations are also utilized by many surface reconstruction algorithms which rely on generation of some distance-like function whose zero set approximates the input points. Construction methods for such functions include the blending of implicit primitives like blobs, spheres, quadrics, and local quadratics that have been fit to the points [14, 12, 15]. For reconstruction, others have used radial basis functions with both global [39] and compact support [26, 10], as well as level set methods [40, 16]. Each of these methods offers various degrees of control on the accuracy with which geometry is represented. Others have used a spatial grid of (usually) trivariate B-splines to represent scalar fields whose zero-sets represent the boundary of sculpted geometry [18, 27].

Many of the above methods and representations may be adapted for field modeling. We will demonstrate the advantages of the proposed approach using approximate distance fields represented in terms of a geometrically non-conforming grid of basis functions fit to samples of exact distance or other distance-like function. For field modeling problems with Dirichlet boundary conditions, the approximate distance field must possess non-zero gradient everywhere on it's zero set. In addition, Neumann and mixed boundary conditions require the magnitude of the gradient to be precisely one at the zero set. Through distance sampling, we can unify field modeling on all geometric models, while bypassing many computational difficulties often associated with exact distance fields, including non-differentiability and lack of local support. By choosing the resolution of the approximate distance field fit to the samples, the accuracy of the geometric approximation to the original geometry is easily controlled. Furthermore, the accuracy of the field solution can be controlled separately to gain solution speed at the expense of accuracy. We demonstrate the generality of our approach by performing analysis on a selection of geometric data sources with a variety of boundary conditions, including boundary conditions that are transient and moving.

2 Homogeneous Dirichlet Boundary Condition

Following Kantorovich [9], a field u that is subject to the homogeneous Dirichlet boundary condition

$$u_{|\partial\Omega} = 0 \tag{1}$$

may be represented as the product of two functions

$$u = \omega\Phi. \tag{2}$$

We now examine the components of this expression in more detail below. Function ω is used to satisfy and to extend the homogeneous Dirichlet boundary conditions into the interior domain; it must have non-vanishing gradient on the boundary of the domain, $\partial\Omega$, where $\omega = 0$. These properties are clearly satisfied by approximate distance fields, and, therefore, they can be chosen to represent ω in expression (2). If the shape of a geometric object is known a priori, such a function can be constructed by a variety of methods [1, 3, 4, 20, 32]. For a geometric object described by a distance field sampled at scattered points, we construct an approximate distance field ω from the sample data, using any of the known fitting methods. In this particular case, we represent an approximate distance field ω by a linear combination of basis functions:

$$\omega = \sum_{i=1}^{m} C_i^{\omega} \chi_i^{\omega}, \tag{3}$$

where the C_i^{ω} are the coefficients of the m basis functions χ_i^{ω} of the spatial variables (x, y, z). For our implementation, we chose χ_i^{ω} as multi-variate B-splines, usually arranged on a regular Cartesian grid. (See [5] for details.)

The type and resolution of sampling, as well as the approximation properties of these basis functions, determine the accuracy of the constructed field. For example, some (but not all) sampling techniques may require signed distance

fields in order to assure the non-vanishing gradient and capture the geometric detail at the domain's boundary. Detailed investigation of these approximation properties is outside the scope of this paper. We note, however, that the zero set of the constructed distance field approximates the boundary of the geometric domain; hence the choice of basis functions, $\{\chi_i^\omega\}_{i=1}^m$, gives direct control of the level of geometric detail in the represented geometric domain. We will explore this capability through examples in Sections 4 and 6.

The second function in expression (2) — function Φ — provides the degrees of freedom that allow to satisfy additional constraints prescribed on u, typically in the form of a differential or integral equation. In most practical situations Φ cannot be determined exactly, and therefore it is represented by *another* linear combination of basis functions:

$$\Phi = \sum_{i=1}^{n} C_i^\Phi \chi_i^\Phi, \tag{4}$$

where the C_i^ϕ are the coefficients of the n basis functions, χ_i^ϕ, of the spatial variables (x, y, z). Popular choices of χ_i^ϕ include B-splines, polynomials, and radial basis functions.

Substituting expressions (3) and (4) into (2) we obtain a new form of Kantorovich's representation for u:

$$u = \left(\sum_{i=1}^{m} C_i^\omega \chi_i^\omega\right)\left(\sum_{j=1}^{n} C_j^\Phi \chi_j^\Phi\right) = \sum_{i=1}^{m}\sum_{j=1}^{n} C_i^\omega \chi_i^\omega C_j^\Phi \chi_j^\Phi. \tag{5}$$

This last expression contains two independent systems of basis functions, $\{\chi_i^\Phi\}_{i=1}^n$ and $\{\chi_i^\omega\}_{i=1}^m$, each serving specific and distinct purposes. Basis functions $\{\chi_i^\omega\}_{i=1}^m$ together with coefficients $\{C_i^\omega\}_{i=1}^m$ are used to approximate a distance field to the boundary of a geometric model. The accuracy of the boundary approximation by the zero set of an approximate distance field governs the accuracy of the treatment of the specified boundary conditions. By construction, the function u represented either by expression (2) or (5) satisfies boundary condition (1) exactly on the zero set of the distance field ω.

The sole purpose of basis functions $\{\chi_i^\Phi\}_{i=1}^n$ is to provide the necessary degrees of freedom to accommodate, as closely as possible, the additional constraints on u. Numerical values of the coefficients $\{C_i^\Phi\}_{i=1}^n$ are determined by a solution procedure which typically consists of application of a variational or projection method with subsequent solution of an algebraic problem. The choice of a particular solution method depends primarily on the type of additional constraints on u. If several solution methods are available for the given type of problem, preference is given to the methods that provide better convergence. Further, the numbers of basis functions, m and n, *independently* control the respective accuracies of the geometric approximation and the solution to the differential equation.

Figure 2 shows application of the described method to the solution of a Poisson equation

$$\nabla^2 u = -q \tag{6}$$

with homogeneous Dirichlet boundary conditions (1) prescribed on the surface of a mannequin head and $q = 1$ taking on a constant value of 1. The head is originally represented by a set of scattered surface points or a surface mesh (Figure 3(a)). In order to satisfy the prescribed boundary condition, first we construct an approximate distance field whose zero set corresponds to the surface of the head. For this construction we employ tricubic B-splines defined over a uniform $61 \times 61 \times 61$ cartesian grid. The computed distance field is shown in Figure 3(b); the coefficients $\{C_i^\omega\}$ being determined by a least square fit to approximately 3.4 million randomly distributed distance samples.

The least square fit to the distance samples requires the minimization of the following functional:

$$F = \sum_{j=1}^{k}\left(\sum_{i=1}^{m} C_i^\omega \chi_i^\omega - d_j\right)^2, \tag{7}$$

where k is the number of distance samples, and d_j is the j^{th} sample taken at the point (x_j, y_j, z_j). This leads to the following linear system:

$$\mathbf{A}\mathbf{C}^\omega = \mathbf{B}, \tag{8}$$

with matrix elements assigned as follows:

$$a_{i,j} = \sum_{l=1}^{k} \chi_i^\omega(x_l, y_l, z_l)\chi_j^\omega(x_l, y_l, z_l), \tag{9}$$

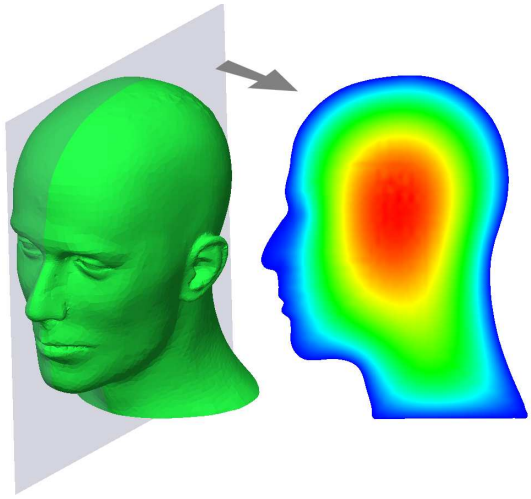

Figure 2: Distribution of the function u that satisfies homogeneous Dirichlet boundary condition (1) on the zero set of the approximate distance field shown in Figure 3(b) and approximates solution of Poisson equation (6).

and

$$b_i = \sum_{l=1}^{k} d_l \chi_i^{\omega}(x_l, y_l, z_l). \tag{10}$$

In order to find a function u that gives the best approximation to equation (6), while satisfying boundary condition (1), we use a classical Ritz method [19, 13] which requires minimization of the functional:

$$F = \iiint_{\Omega} u(\nabla^2 u) d\Omega - 2 \iiint_{\Omega} u(-q) d\Omega.$$

Employing a Ritz method reduces the original boundary value problem to the solution of a system of linear algebraic equations: $\mathbf{A}\mathbf{C}^{\Phi} = \mathbf{B}$, where $\mathbf{C}^{\Phi}$ is a vector of unknown coefficients of the basis functions, and the elements of matrix $\mathbf{A}$ and vector $\mathbf{B}$ are computed through the following triple integrals:

$$\begin{aligned} a_{ij} &= \iiint_{\Omega} \nabla \left(\sum_{k=1}^{m} C_k^{\omega} \chi_k^{\omega} \chi_i^{\Phi} \right) \nabla \left(\sum_{l=1}^{m} C_l^{\omega} \chi_l^{\omega} \chi_j^{\Phi} \right) d\Omega; \\ b_i &= \iiint_{\Omega} q \left(\sum_{k=1}^{m} C_k^{\omega} \chi_k^{\omega} \chi_i^{\Phi} \right) d\Omega. \end{aligned} \tag{11}$$

For more details, please refer to the Appendix, where the derivation of the linear system for a Dirichlet boundary value problem is provided.

The solution in Figure 2 was computed by choosing the basis functions $\{\chi_i^{\Phi}\}_{i=1}^{n}$ to be trilinear B-splines on a $41 \times 41 \times 41$ uniform Cartesian grid. Volumetric integration is performed over the supports of the B-splines using Gaussian cubature rules to allocate the integration points. To assure that all integration points are allocated only inside the domain, hierarchical space decomposition and marching cubes techniques are employed as described in [36]. Figure 2 shows the distribution of the computed function u in the middle cross-section of the mannequin head. The function satisfies the homogeneous Dirichlet boundary condition (1) exactly on the zero set of the approximate distance field shown in Figure 3(b) and approximates the solution of the Poisson equation (6). Despite trilinear B-splines having discontinuous first order derivatives, they constitute an admissible space of functions for approximating the solution of the boundary value problems in equations (6) and (1) [35]. The continuous variation of hue corresponds to continuous variation of the function from zero on the boundary (blue color) to its maximum value of 14.94 shown

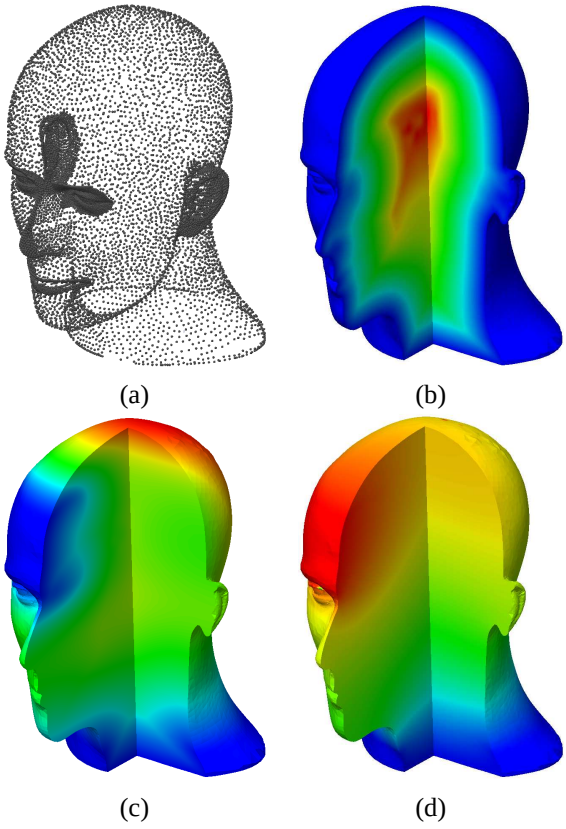

Figure 3: Modeling of temperature field in mannequin head: (a) scattered points on the surface of the head generated by 3D scanner; (b) constructed approximate distance field; (c) an approximate distance field to portions of the boundary where the value of temperature is prescribed; (d) distribution of temperature that satisfies the boundary conditions exactly.

in red. The images in this example, as well as those in the remainder of this paper, are computed by sampling the solution field over the boundary of the geometric domain.[1]

3 Non-Homogeneous Dirichlet Boundary Conditions

Treatment of the non-homogeneous Dirichlet boundary condition:

$$u_{|\partial\Omega} = \varphi, \tag{12}$$

where the function φ is a priori known function of spatial coordinates, requires just a slight modification of Kantorovich's method. Since the function u, given by expression (5), already satisfies the homogeneous boundary condition (1), the addition of the function φ to expression (5) turns u into a family of functions that satisfy boundary condition (12) exactly:

$$u = \sum_{i=1}^{m} \sum_{j=1}^{n} C_i^{\omega} \chi_i^{\omega} C_j^{\Phi} \chi_j^{\Phi} + \varphi. \tag{13}$$

[1] In this particular case, the boundary is represented by a triangular surface mesh. To improve the efficiency of the display process, the solution field might also have an intermediate representation as a dense, uniform lattice of solution samples. The values from this lattice are then trilinearly interpolated for display.

To extract a particular function from this family we need to impose additional constraints on u. For instance, we can require the function u to be an approximate solution of the Laplace equation:

$$\nabla^2 u = 0. \tag{14}$$

Using this condition we can compute numerical values of the coefficients $\{C_i^\Phi\}_{i=1}^n$ in expression (13). To solve the problem, we again employ a Ritz method that leads to the solution of an algebraic system, $\mathbf{AC}^\Phi = \mathbf{B}$, where the elements a_{ij} of matrix $\mathbf{A}$ are computed using expression (11), previously used to solve a Poisson equation with homogeneous Dirichlet boundary condition. Elements of vector $\mathbf{B}$ are given by the following integrals:

$$b_i = -\iiint_\Omega \nabla\varphi\nabla\left(\sum_{k=1}^{m} C_k^\omega \chi_k^\omega \chi_i^\Phi\right) d\Omega. \tag{15}$$

Once the coefficients $\{C_i^\Phi\}_{i=1}^n$ are determined, u can be evaluated at any given point in the domain.

Since the formulation contains a product of approximate distance and some set of basis functions, the basis functions for the solution must be able to attenuate the approximate distance while also representing the solution field. Our experience suggests that representing the approximate distance on the same resolution grid as the solution field is commonly acceptable, but we explore different combinations of grid resolution below and in Section 4. Figure 4(b) shows the distribution of u, approximating Laplace equation (14) and satisfying non-homogeneous Dirichlet boundary condition (12) with

$$\begin{aligned}\varphi(x,y,z) = & cos\left(\frac{10\pi(x-x_{min})}{x_{max}-x_{min}}\right) cos\left(\frac{10\pi(y-y_{min})}{y_{max}-y_{min}}\right) \\ & cos\left(\frac{15\pi(z-z_{min})}{z_{max}-z_{min}}\right).\end{aligned} \tag{16}$$

The approximate distance field is the same as we used in the last section to solve the problem with homogeneous boundary conditions. It is represented by a linear combination of tricubic splines on a $61 \times 61 \times 61$ Cartesian grid with coefficients determined by a least square fit to 3.4 million randomly distributed samples of distance. The basis functions $\{\chi_i^\Phi\}_{i=1}^n$ that approximate the solution are trilinear B-splines on a $41 \times 41 \times 41$ Cartesian grid. As shown in Figure 4(b), these basis functions provide sufficient degrees of freedom to attenuate the influence of the periodic boundary condition (16) away from the zero set of the approximate distance field.

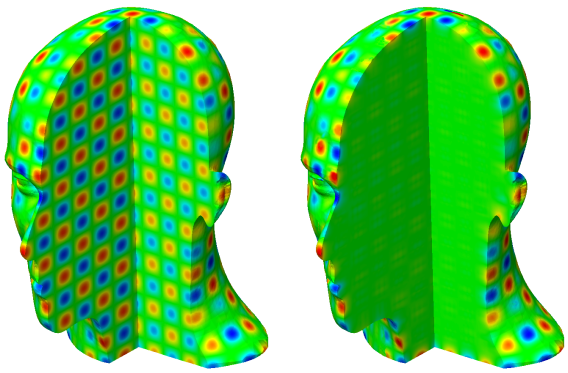

(a) (b)

Figure 4: (a) Distribution of a periodic function φ (16) prescribed as a boundary condition for Laplace equation (14); (b) solution of Laplace equation that satisfies Dirichlet boundary condition given by a function shown in (a). Notice that basis functions provide sufficient degrees of freedom to attenuate the influence of periodic boundary condition (16) away from the zero set of the approximate distance field.

In general, a boundary condition function φ may not be known explicitly or is not prescribed *globally*. More typically, the boundary conditions are prescribed in a piecewise manner, i.e. the boundary conditions are specified by

individual functions φ_i on each portion of boundary, $\partial\Omega_i$:

$$u_{|\partial\Omega_i} = \varphi_i, \quad i = 1, N. \tag{17}$$

In this case the field u that satisfies Dirichlet boundary conditions (17) can still be represented by expression (13), but the function φ must be constructed in such a way that on every boundary segment, $\partial\Omega_i$, it coincides with the prescribed function φ_i. One could use a variety of methods, including sampling, but we choose to construct function φ using transfinite interpolation [23], a technique that can be considered to be an extension of inverse distance weighted interpolation [34]. The interpolating function is represented by a weighted sum of functions prescribed on the boundaries $\varphi = \sum_{i=1}^{N} \varphi_i W_i$; with weights, W_i, inversely proportional to the distances to the boundaries, $\partial\Omega_i$:

$$W_i = \frac{\omega_i^{-\mu_i}}{\sum_{j=1}^{N} \omega_j^{-\mu_j}}. \tag{18}$$

The expression for the weights, W_i, can be rewritten in a numerically stable form, more suitable for implementation in software:

$$W_i = \frac{\prod_{j=1;j\neq i}^{N} \omega_j^{\mu_j}}{\sum_{k=1}^{N} \prod_{j=1;j\neq k}^{N} \omega_j^{\mu_j}}. \tag{19}$$

As before, the functions ω_i are approximate distance fields to the partial boundaries $\partial\Omega_i$. Exponents μ_i in the expression for the weights W_i affect behavior of the weights in the neighborhoods of the zero sets of the approximate distance fields ω_i. Values of μ_i greater than one are used to interpolate normal derivatives prescribed on $\partial\Omega_i$. In this case the value of μ_i must be one greater than the order of the prescribed derivatives. (The readers are referred to [23] for additional details.)

Let us construct a function that interpolates temperature values of $35°C$ and $40°C$ prescribed on the neck and forehead of the mannequin head respectively. The interpolating function φ, whose distribution is shown in Figure 5(d), then appears as follows:

$$\varphi = \frac{35\omega_2}{\omega_1 + \omega_2} + \frac{40\omega_1}{\omega_1 + \omega_2}, \tag{20}$$

where ω_1 and ω_2 are approximate distance fields to the neck (Figure 5(b)) and the forehead (Figure 5(c)). These fields to individual boundary segments are constructed by trimming the distance field to the whole surface of the head using the normalized trimming method described in [32]. Once the interpolating function φ is constructed it is substituted into expression (13). Approximation of the additional constraints, involves application of a solution procedure similar to that described above to determine numerical values for the coefficients C_i^{Φ}. Note that the union of boundary segments where Dirichlet boundary conditions are specified does not constitute the complete boundary of the geometric domain, and therefore the function ω in the Taylor series expansion

$$u = \omega \sum_{i=1}^{n} C_i^{\Phi} \chi_i^{\Phi} + \varphi \tag{21}$$

is an approximate distance field to the union of the boundaries where different Dirichlet boundary conditions are specified. Figure 3(c) shows the composite approximate distance field ω to the union of forehead and the mannequin neck. This approximate distance field is constructed from individual distance fields to the forehead ω_1 and the neck ω_2 using s joining R-function: $\omega_1 + \omega_2 - \sqrt{\omega_1^2 + \omega_2^2}$ [20, 28]. Other joining techniques may be also used as described in [32, 3]. Figure 3(d) illustrates the distribution of a function u that takes on prescribed values of 35 and 40 on the neck and forehead respectively and approximates the solution of Laplace equation (14) everywhere in the domain. A Ritz method is used to determine the coefficients C_i^{Φ} of trilinear B-splines $\{\chi_i^{\Phi}\}$ defined on a uniform $41 \times 41 \times 41$ Cartesian grid.

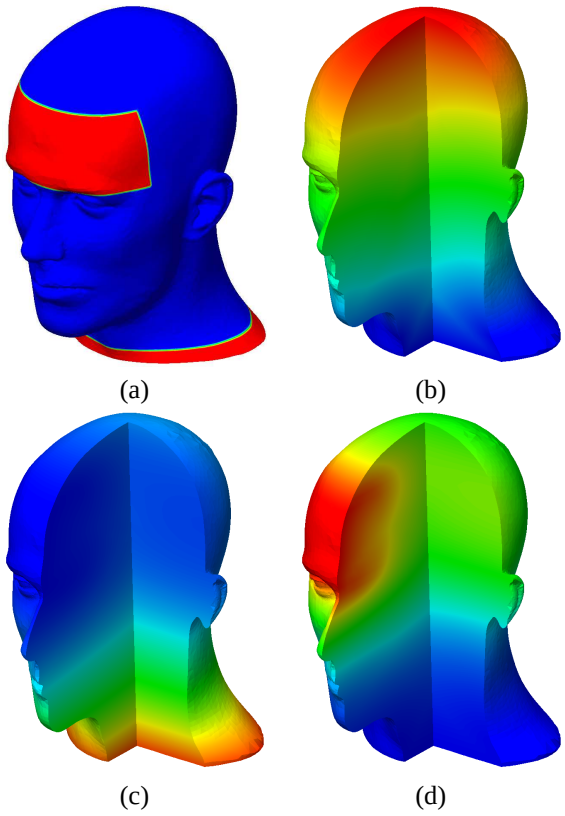

Figure 5: (a) Red colored zones depict the portions of the surface of the head where the values of temperature are specified; (b) hue values correspond to approximate distance to the lower part of the neck; (c) hue values correspond to approximate distance to the forehead; (d) distribution of function, (20), that interpolates temperature values of $35°C$ and $40°C$ prescribed on the neck and forehead respectively.

4 General Boundary Conditions with Resolution Control

Kantorovich's idea to satisfy Dirichlet boundary conditions advanced the variational methods with the ability to satisfy essential boundary conditions exactly and concentrate the power of the solution method on approximation of the differential equation for the boundary value problem. Rvachev and his students generalized Kantorovich's method to satisfy other types of boundary conditions exactly by representing a field u by a generalized Taylor series of powers of a *normalized* distance field. An approximate distance field ω is called *normalized* to the order m with respect to domain Ω if it satisfies the following conditions:

$$\omega|_{\partial\Omega} = 0; \quad \frac{\partial\omega}{\partial n}|_{\partial\Omega} = 1; \quad \frac{\partial^k\omega}{\partial n^k}|_{\partial\Omega} = 0, \quad k = 2, \ldots, m,$$

where n is the vector normal to the boundary $\partial\Omega$. Intuitively, normalized distance fields approximate the exact distance functions to the order m near the boundary of the domain. If such a function ω is known for a given domain Ω, any field over Ω can be represented by a Taylor series expansion in the vicinity of the boundary $\partial\Omega$ as [20, 22]:

$$u = u_0(0) + \sum_{k=1}^{m} \frac{1}{k!} u_k(0)\omega^k + O\left(\omega^{m+1}\right), \tag{22}$$

In this case, each $u_k(0)$, $k = 0, \ldots, m$ corresponds to the normal derivative of kth order on the boundary $\partial\Omega$. In [22], the authors proved the completeness of the representation of fields by a power series of normalized distance

field (22). An important consequence of the completeness theorem is that the remainder term in the series (22) may be represented to arbitrary precision by a product of the $(m+1)$st power of a normalized distance field ω and a polynomial Φ: $O\left(\omega^{m+1}\right) = \omega^{m+1}\Phi$.

Using the generalized Taylor series (22) one can easily and systematically derive expressions for functions satisfying different kinds of boundary conditions. For example, the expression

$$u = \underbrace{\left(\Phi_1 - \omega\nabla\omega\cdot\nabla\Phi_1\right)}_{u_0(0)} + \underbrace{\left(\psi - h\Phi_1\right)\omega}_{u_1(0)\omega} + \underbrace{\omega^2\Phi_2}_{O(\omega^2)} \tag{23}$$

defines a family of functions that satisfy the following boundary condition:

$$\left(\frac{\partial u}{\partial n} + hu\right)\Big|_{\partial\Omega} = \psi. \tag{24}$$

The first term u_0 in expression (23) represents a value of the function prescribed on the boundary $\partial\Omega$. Since boundary condition (24) does not explicitly prescribe the value of u on the boundary, u_0 is represented by a linear combination of basis functions $\Phi_1 = \sum_{i=1}^{n} C_i^{\Phi_1}\chi_i^{\Phi_1}$ with undetermined coefficients $C_i^{\Phi_1}$. Subtraction of $\omega\nabla\omega\cdot\nabla\Phi_1$ from Φ_1 ensures that the first normal derivative of u_0 vanishes on the zero set of ω [20, 22]. The second term in expression (23) represents a first order normal derivative of u whose value on the boundary $\partial\Omega$ is derived from the boundary condition (24): $\frac{\partial u}{\partial n}\big|_{\partial\Omega} = \psi - hu$. The remainder term $\omega^2\Phi_2$ guarantees completeness of u. Similar to a Dirichlet boundary condition, if different functions h_i and ψ_i have been specified on different portions of the boundary, these functions are transfinitely interpolated using the approximate distance fields for each boundary segment [23], and are then substituted into the generalized Taylor series (23). Taylor series expansion (22) implies a similar procedure for every possible type of boundary conditions, and expressions for most common boundary value problems have already been derived[20, 21].

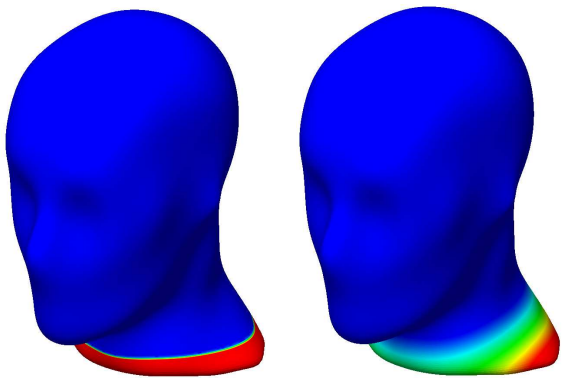

(a) (b)

Figure 6: (a) Zero set of an approximate distance field represented by a linear combination of tricubic B-splines defined on a $10\times10\times10$ grid with prescribed Neumann boundary condition $\frac{\partial u}{\partial n}|_{\partial\Omega_1} = -1$ (red) and the boundary condition $\left(\frac{\partial u}{\partial n} + 0.1u\right)|_{\partial\Omega_2} = 27.3$ (blue); (b) distribution of the solution of Laplace equation that satisfies prescribed boundary conditions shown in (a).

The modeling methods described in this paper are based on the observation that normalized distance field can be also approximated by fields generated from sampled data. Therefore such approximate distance fields can be used to construct functions that satisfy general boundary conditions. If an approximate distance field is not normalized, but possesses non-vanishing gradient on its zero set, it can be normalized to any order as described in [20, 3]. Furthermore, each Taylor series expansion contains two types of approximated functions: distance functions ω_i and unknown functions Φ_i, effectively factoring the resolution of the field problem into *geometric* and *physical* accuracy respectively.

Most engineering analyses require *defeaturing* of geometric models before they can be used for analysis and simulation. This process manually removes unwanted geometric details, small features, and other problematic geometry;

and usually requires substantial judgement and expertise. Through the use of approximate distance fields represented with different spatial resolutions, a basic exploration of automatic defeaturing is possible. In its simplest form, defeaturing by resolution control will globally remove unnecessary details or noise from the initial geometry by a smooth approximation of the distance field. For example, a plot of the zero set of an approximate distance field represented by a linear combination of tricubic B-splines defined on a $10 \times 10 \times 10$ grid is shown in Figure 6(a). Using a coarser grid results in the smooth approximation of facial features, providing a natural means to support automatic defeaturing.

More sophisticated control of approximate distance fields enable greater control of the defeaturing process. For example, non-uniform grids of basis functions would enable local variation and control of resolution. Another approach would have selected distance samples assigned greater priority in a *weighted* least squares fit. Further adaptive techniques from reconstruction methods can provide flexible control of the geometric resolution of the approximate distance field [15]. Figure 6(a) shows that the nose, ears and eyes have been smoothed out by the zero isosurface of the approximate distance field. Figure 6(b) presents the distribution of a function that approximates the solution of Laplace equation (14) and satisfies Neumann boundary condition $\frac{\partial u}{\partial n}|_{\partial\Omega_1} = -1$ on the mannequin neck (shown in red in Figure 6(a)). On the rest of the head's surface (blue region in Figure 6(a)), the boundary condition $\left(\frac{\partial u}{\partial n} + 0.1u\right)|_{\partial\Omega_2} = 27.3$ is applied. The prescribed boundary conditions are represented by one expression $\left(\frac{\partial u}{\partial n} + hu\right)|_{\partial\Omega} = \psi$, where the function h transfinitely interpolates values of 0 and 0.1 prescribed over the red and blue zones in Figure 6(a); function ψ transfinitely interpolates values of -1 and 27.3 prescribed over the same surface segments. The solution of the problem is represented by expression (23) in which the basis functions $\{\chi_i^{\Phi_1}\}$ and $\{\chi_i^{\Phi_2}\}$ have been chosen to be polynomials of degree 7. In this example, coefficients of both sets of basis functions, C_i^{Φ}, are determined by the least square method. The essential boundary condition (24) is enforced *exactly* for a function u represented by the generalized Taylor series (23), and the least square method handles approximation of the differential equation only.

Similarly, physical resolution of the field may be controlled separately by approximation of the unknown functions Φ_i. Physical resolution is characterized by the ability of the basis functions to capture high gradients, curvature and other singularities in a physical field. In Figure 7 the analysis results from several combinations of grid resolutions are depicted. Figure 7(a) and (b) represent geometry with a coarse grid while incorporating a fine grid for representation of the physical field. This combination of low geometric resolution and high physical resolution had a total running time of 6 hours, 34 minutes. Figure 7(c), on the other hand, has high geometric resolution and low field resolution, and total running time of 43 minutes. The images reveal artifacts in (c) where there are insufficient degrees of freedom to approximate the differential equation precisely. By contrast, the fully automated solution procedure for the example with homogeneous boundary conditions in Figure 2 took 6 hours, 55 minutes at the described resolution. Solution of a similar problem with more complex, non-homogeneous Dirichlet boundary conditions in Figure 3(d) required 13 hours, 19 minutes.

Such use of independent geometric and physical grids at different resolutions leads to modular separation of geometric and physical accuracies using two or more sets of basis functions. Furthermore, resolution of each boundary condition may be also controlled separately since each boundary condition is associated with its own Taylor series expansion, and its own distance field. This unique feature of our approach provides powerful controls for controlling resolution of field modeling that is not possible with traditional mesh-based methods.

5 Applications and Examples

The field modeling method we discussed in this paper has been used previously quite extensively with implicit geometric representations constructed using R-functions. The R-function method has been applied to problems in heat transfer, structural analysis, plate bending, plate vibration, and fluid dynamics, among others [24, 25, 38, 21]. A general architecture of a meshfree field modeling and simulation system based on distance fields is described in [36], and fully functional two-dimensional prototype software may be downloaded from http://sal-cnc.me.wisc.edu. The present research establishes that we can solve all these problems and more with other types of approximate distance fields, in particular those constructed from sampled data. Practical consequences of this observation include easier implementation, higher level of automation, improved speed, and automated variable resolution control. Below we demonstrate the power of the method with two non-trivial applications. The fully automated, but fairly brute-force, solution procedures described in this paper have solution times ranging from tens of minutes to tens of hours on a dual processor 1GHz Pentium III workstation with 1.5GB RAM. The solution procedure includes integrating, assembling, and solving the linear system for the unknown coefficients C_i^{Φ} of the basis functions χ_i^{Φ}, and is dominated by

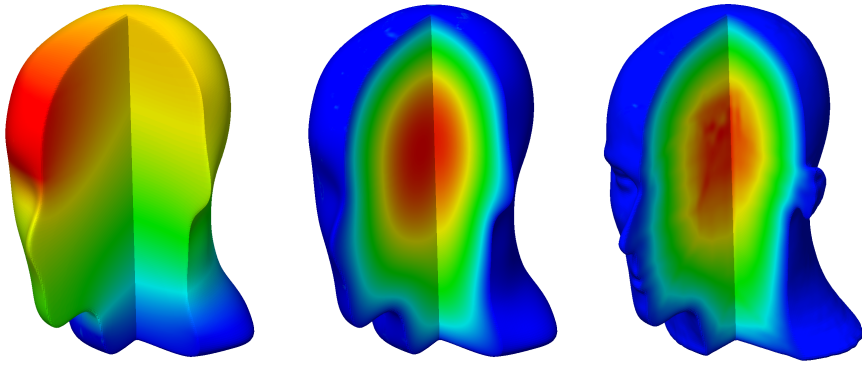

(a) (b) (c)

Figure 7: (a) A temperature distribution modeled using tricubic B-splines on a $10 \times 10 \times 10$ grid to approximate the geometry and a $41 \times 41 \times 41$ grid for the solution. (b) Solution of Poisson equation (6) with homogeneous Dirichlet boundary conditions. Distance field is represented by a linear combination of tricubic B-splines on a $10 \times 10 \times 10$ grid. Solution is approximated with trilinear B-splines on a higher resolution, $41 \times 41 \times 41$ grid. (c) Solution of the same problem with approximate distance field represented by a linear combination of tricubic B-splines on $61 \times 61 \times 61$ grid and solution computed on a lower resolution $14 \times 14 \times 19$ grid of trilinear B-splines.

the numerical integration over the domain to construct the linear system. Sampling of the distance field, fitting, and visualization constitute a small fraction of the total solution time. As we explained in the last section and demonstrate below, the running times depend largely on complexity of boundary conditions and desired geometric or physical resolution.

5.1 Scan and Solve

The use of distance fields derived from sampled data makes it possible to implement a "scan-and-solve" approach to modeling of physical fields, which is particularly effective when physical fields need to be modeled and analyzed in existing artifacts for which traditional geometric models may not exist. Reverse engineering of geometric models for such parts is a difficult and time consuming process fraught with difficulties due to inaccuracies, wear, deformations, and imprecision of both natural and engineered objects. The key observation is that the traditional reverse engineering and meshing pipeline may be bypassed if an object model and its boundary are described by an approximate distance field. Such fields may be often constructed directly from sampled data generated by 3D laser scanners or other scanning technology. Once the points on the surface of the part have been generated, a variety of methods can be used to compute an approximate distance field. In our examples the exact distance field was randomly sampled throughout the volume, and then represented by B-splines with coefficients computed using the least square method.

The "scan and solve" approach is depicted in the flowchart in Figure 8, with operands depicted as ovals, and operations depicted as rectangles. At the outset, the geometry is scanned to produce a 2 or 3 dimensional image. Here *image* refers to a regular grid of pixels or voxels for 2D or 3D geometry, respectively. The image is then segmented using image processing techniques to produce a binary image with foreground and background only. A Euclidean distance transform [11] is then applied to compute a distance value for each image element. Samples of the distance image are taken at randomly distributed points and a set of basis functions are fit to these samples to produce an approximate distance field. The approximate distance field is then used to support meshfree simulation of stress or other physical quantities.

As a demonstration of the "scan and solve" approach, Figure 9 shows two-dimensional stress analysis performed on a scanned model of a wrench. Applicability of the meshfree method with R-functions to problems in elasticity has been demonstrated previously in [24]. Here we extend the method to incorporate approximate distance fields computed from image data. Figure 9(d) shows a plot of an approximate distance field constructed by a least square fit to the sampled exact distance field in Figure 9(c), using bicubic B-splines on a uniform 61×181 grid. The exact distance to the boundary of a scanned image of a wrench was computed by the sequential Euclidean distance

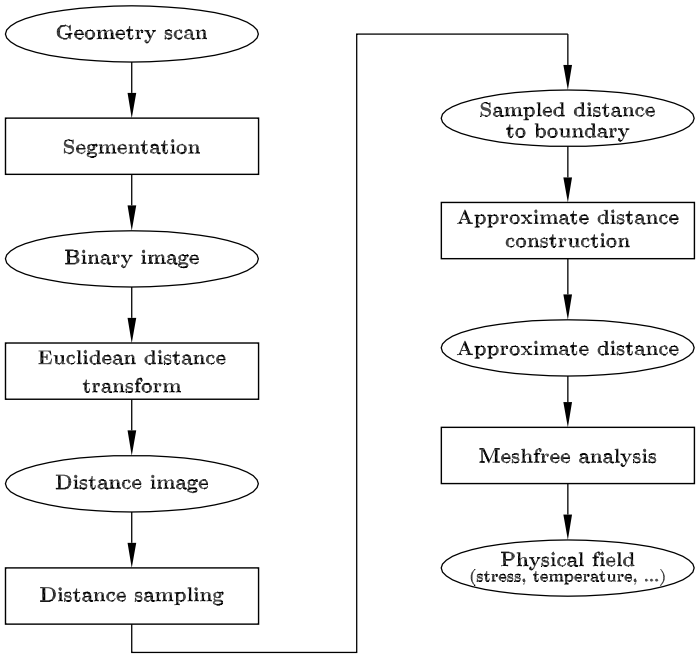

Figure 8: This figure shows the typical scheme for the "scan and solve" type of stress analysis.

transform. The displacement and loading boundary conditions on the wrench are shown in Figure 9(g) which also shows the computed principal normal stress σ_1 in the wrench. In order to apply the boundary conditions, the distance fields to the corresponding portions of boundary were constructed by normalized trimming [32] of the approximate distance field of the wrench in Figure 9(d). Figure 9(f) shows a portion of the distance field to the fixed boundary. The solution procedure combines these distance fields and another system of B-splines into generalized Taylor series that represent components of the displacement vector field, $\{u, v\}$, where $u = \omega\Phi_u$ and $v = \omega\Phi_v$ (one scalar series for each scalar component of the displacement field). By minimizing the potential energy of elastic deformation, we compute numerical values of the undetermined coefficients in these Taylor series. Once the displacement field has been determined, stresses inside the wrench body are computed using standard automatic differentiation tools. Figure 9(g) presents a plot of principal normal stress σ_1 in the wrench. At no steps did the solution procedure require boundary representation, meshing, or other topological reconstructions. The total solution time for this example is 22 minutes, 17 seconds.

5.2 Sample and Solve

Sampling is a promising alternative even when the geometric model (e.g. boundary representation) of the domain is available, as in the case of most mechanical components and systems. In this case, "sample-and-solve" could be an effective method for dealing with complexity and resolution of complex engineering systems. The strategy is similar to "scan-and-solve," except that the approximate distance field is not constructed from scanned data, but may be be sampled at desired resolution from the given geometric model.

Figures 10 and 11 demonstrate one such example, involving modeling of transient temperature field in a truck brake assembly (Figure 10(a)). The example components were designed in a commercial solid modeling system, but automatic meshing tools were not able to produce a mesh due to "small geometric features". Even with perfect geometric models, this problem is challenging for mesh-based methods because the spatial mesh has to account for the rotation of the disk. Thus, cells located in the pads have to be aligned with cells located in the disk at every time slice. This condition makes the meshing substantially more difficult and often restricts relative motion of the parts [33]. The meshfree computational technology we discuss here does not impose such conditions on the grids of basis

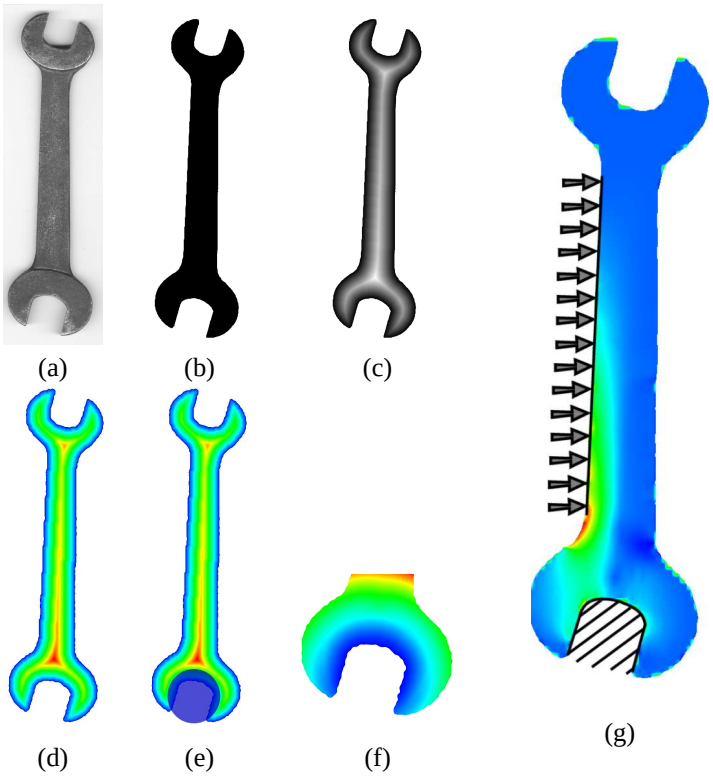

Figure 9: The sequence of analysis for "scan and solve" starts with (a) a 2D scan of the specimen. (b) The image is processed to produce a binary image of the wrench. (c) The sequential Euclidean distance transformation is applied to compute the distance to the boundary at every pixel. (d) Samples of distance are taken over the transformed image and an approximate distance field, represented by a grid of bicubic B-splines, is fit to the samples. (e) A normalized trimming operation[32] is performed to produce the distance field, shown partially in (f), for the fixed boundary condition. (g) The system is solved and the principal normal stress σ_1 is derived from the computed displacement field.

functions. In fact, the same grid of basis functions can be used at every time step. For simplicity, let us assume that all parts of the assembly are made from the same material (iron) with thermal conductivity $\lambda = 47.7W/(m \cdot K)$, specific heat $c = 490J/(kg \cdot K)$, and specific mass $\rho = 7850kg/m^3$. The initial temperature of the assembly is $30°C$. We model the heat generation due to application of the brake pads to the disk by placing volumetric heat sources $q_v = 93.199 \cdot 10^6 W/m^3$ into the pads. The external surface of the assembly is cooled by air with temperature of $30°C$. The intensity of the convective cooling is described by the convective coefficient $\alpha = 50W/(m^2 \cdot K)$ applied to all exposed surfaces.

The sample-and-solve solution procedure requires three distance fields: a distance field that describes the external surface of the brake assembly (Figure 10(b)) – to construct a temperature field satisfying the convective boundary conditions; a distance field that describes internal points of the brake pads (Figure 10(c)) – in order to specify heat sources; and a distance field that describes the interior of the disk (Figure 10(d)) – in order to accommodate its rotation. These distance fields were constructed using different grids of B-splines, depending on their role in the solution procedure: triquintic B-splines over a $65 \times 65 \times 25$ Cartesian grid for the assembly, and trilinear B-splines over a $100 \times 100 \times 80$ Cartesian grid for the pads and rotor. The grids of trilinear B-splines served to define the domains for integration. The rotation of the disk was accommodated in the problem formulation by backward differences (in time) to prior solutions, using spatial transformation (according to disk rotation) of quadrature points lying within the disk. The computed temperature distributions at the first six time steps are shown in Figure 11. The temperature was represented by expression (23) with the functions Φ_1 and Φ_2 approximated by linear combinations of tricubic B-splines over a $45 \times 45 \times 25$ Cartesian grid. The coefficients $C_i^{\Phi_1}$ and $C_i^{\Phi_2}$ were determined by application of the least square

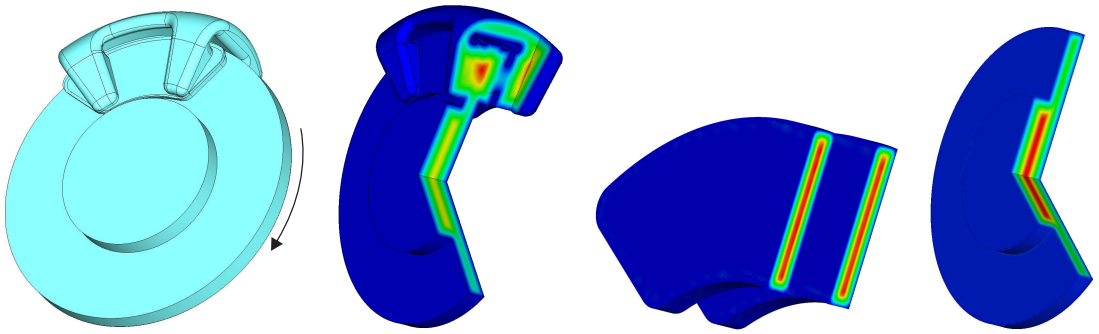

(a) (b) (c) (d)

Figure 10: (a) A truck brake assembly. Approximate distance fields to the boundaries of (b) brake assembly, (c) brake pads, and (d) the disk.

method to the time-discretized heat conduction equation. Note that boundary conditions of convective heat exchange are essential with the least square method, and, therefore, the basis functions approximating the temperature field must be constructed using expression (23) that satisfies these conditions. In contrast with previously discussed examples the solution procedure for this problem required computations of third order partial derivatives of the basis functions and the assembly of distance fields, causing the solution time at full resolution to be approximately 65 hours per time step. While this may appear to be computationally expensive in comparison with mesh-based methods, the example clearly demonstrates the feasibility and the power of using sampled distance fields to support meshfree simulations in complex systems.

6 Conclusion

The use of approximate distances has the potential to substantially advance modeling of physical fields with a wide variety of geometric representations. The proposed method provides a unique opportunity to perform meshfree analysis from native CAD models or directly from sampled data, without generation of intermediate (and often artificial) CAD models and geometrically conforming spatial meshes. As depicted in Figure 1, many difficult or even manual steps in the typical analysis pipeline can therefore be bypassed when dealing with captured geometric data. The formulation of the method naturally provides for separate controls of level of geometric details and accuracy of the computed physical field, with boundary conditions satisfied exactly, up to the precision of the distance field itself. Intuitively, the proposed method is a generalization and extension of the implicit distance-field representation of geometry to modeling of physical phenomena. And in fact, the method can work with most existing implicit geometric representations possessing non-vanishing gradients on their zero sets in place of the approximate distance field.

The described meshfree method, and the scan-and-solve approach in particular, have substantial advantages over conventional mesh based methods in situations where the mesh generation is difficult, expensive, or impossible. For example, our experience indicates that satisfactory finite element meshing of the three-dimensional solid models used in this paper, including the triangulated surface model constructed from sampled data as shown in Figure 3(a) and the brake assembly in Figure 10, is a non-trivial task that cannot be fully automated.

Several aspects of the proposed method would benefit from further studies. Whenever the constructed distance field deviates from the exact geometry, this deviation propagates into the solution of the boundary value problem: instead of solving the original problem, we are actually solving a similar but different problem with boundary conditions satisfied exactly on the zero set of the constructed distance field. As a consequence, the precision of the approximate distance field also controls the accuracy of the boundary condition on the true boundary. If the approximate distance field is exact in the neighborhood of the boundary, then the boundary conditions are exact on the true boundary of the domain. The effects of deviation of the distance field from the exact geometry warrants further investigation with respect to the accuracy of boundary conditions. In [3], the issues surrounding the geometric errors are fully explored; however, the effects on the accuracy of boundary conditions have not been quantified.

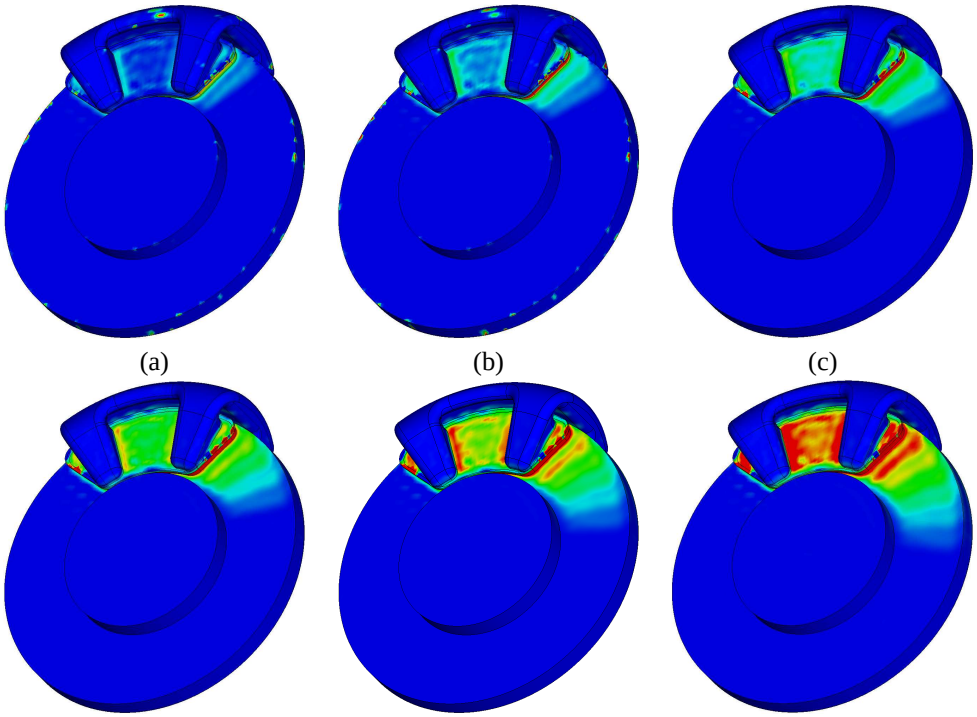

Figure 11: Distributions of transient temperature field in the truck brake assembly computed at first six time steps

A variety of applications appear to be particularly suitable for exploitation of the proposed method. One exciting direction is the extension of the 2D image-based distance and field modeling (recall the wrench example in Section 5.1) to 3D medical data, for example for the structural analysis of bones and implants. Heterogeneous materials and mechanical properties deduced from density information can be incorporated within the modeling procedure in a straightforward fashion [37]. Other promising directions involve adaptive sampling of distance fields for controlled defeaturing, analysis using sampled boundary conditions, and adaptive refinement of physical fields by multi-grid or hierarchical subdivision techniques.

A Detailed Derivation for Dirichlet Conditions

Here we provide a detailed derivation application of the meshfree method with distance fields for solution of a heat transfer problem with Dirichlet boundary conditions. Given a domain, Ω, and temperature on the boundary specified by the function

$$u|_{\partial\Omega} = \varphi, \tag{25}$$

we want to find a temperature distribution, u, that satisfies the Poisson equation,

$$\nabla^2 u = f \tag{26}$$

within the domain. In [9] Kantorovich showed that *any* function satisfying boundary condition (25) can be represented in the following form:

$$u = \varphi + \omega\Phi, \tag{27}$$

where ω is zero on the boundary of the domain and non-zero everywhere else. Function ω is also required to possess non-zero gradient on the boundary $\partial\Omega$ in order to satisfy completeness requirements on u. If ω is an approximate distance field to the boundary, expression (27) is a Taylor series expansion of u by the distance field ω, where φ

specifies the values of u on the boundary and the product $\omega\Phi$ is a remainder term. The purpose of function Φ in the remainder term is to satisfy the additional constraints that have been set on u by the Poisson equation. Since in most practical situations Φ cannot be determined exactly, it is approximated by a linear combination of basis functions:

$$\Phi = \sum_{i=1}^{n} C_i \chi_i. \tag{28}$$

In this case, the solution procedure determines the numerical values of the coefficients $\{C_i\}_{i=1}^n$ that make u the best approximation to the differential equation of the problem.

We substitute the expression for Φ into (27) to get

$$u = \varphi + \omega \sum_{i=1}^{n} C_i \chi_i = \varphi + \sum_{i=1}^{n} C_i \xi_i, \tag{29}$$

where $\xi_i = \omega\chi_i$ are the basis functions satisfying the homogeneous Dirichlet boundary condition on $\partial\Omega$. Since we are looking for a solution of the Poisson equation on the linear space of functions satisfying homogeneous boundary conditions, we need to reformulate the boundary value problem. First, we split u into homogeneous and non-homogeneous parts $u = u_0 + u_1$, where $u_0 = \sum\limits_{i=1}^{n} C_i \xi_i$ and $u_1 = \varphi$. Then we substitute these expressions into the Poisson equation (26) and move all non-homogeneous terms to the right hand side of the equation:

$$\nabla^2 u_0 = f - \nabla^2 u_1. \tag{30}$$

Since Poisson equation (30) with homogeneous Dirichlet boundary condition $u_0|_{\partial\Omega} = 0$ is positive definite, the Ritz method can be used to solve for u_0. The Ritz methods replaces the solution of a differential equation $Au = f$ by an equivalent variational formulation that requires minimization of the following functional:

$$F = (Au, u) - 2(f, u), \tag{31}$$

where A is a differential operator and $(,)$ is the inner product, which for L_2 spaces is $(u, v) = \int_\Omega uv d\Omega$. Applying the Ritz method (31) to the Poisson equation (30) yields the functional:

$$F = \int_\Omega u_0 \nabla^2 u_0 d\Omega - 2\int_\Omega (f - \nabla^2 u_1) u_0 d\Omega. \tag{32}$$

Application of Green's formula to the integrals in this functional allows us to reduce the order of the derivatives in it:

$$F = -\int_\Omega (\nabla u_0)^2 d\Omega - 2\int_\Omega u_0 f d\Omega - 2\int_\Omega \nabla u_1 \cdot \nabla u_0 d\Omega. \tag{33}$$

Substitution of expressions for u_0 and u_1 into functional (33) results in:

$$F = -\int_\Omega \left(\nabla \left(\sum_{j=1}^{n} C_j \xi_j \right) \right)^2 d\Omega - 2\int_\Omega f \sum_{j=1}^{n} C_j \xi_j d\Omega - 2\int_\Omega \nabla\varphi \cdot \nabla \left(\sum_{j=1}^{n} C_j \xi_j \right) d\Omega. \tag{34}$$

To minimize the quadratic functional (34), all partial derivatives of F with respect to the coefficients C_i must vanish:

$$\frac{\partial F}{\partial C_i} = 0, \qquad i = 1, \ldots, n.$$

Differentiating F with respect to C_i gives the expression:

$$\frac{\partial F}{\partial C_i} = -2\int_\Omega \nabla \left(\sum C_j \xi_j \right) \cdot \nabla \xi_i d\Omega - 2\int_\Omega f \xi_i d\Omega - 2\int_\Omega \nabla\varphi \cdot \nabla \xi_i d\Omega.$$

Setting the last expression to zero for $i = 1, \ldots, n$, then rearranging and gathering unknown terms, gives a system of n linear algebraic equations:

$$-\sum_{j=1}^{n} C_j \int_\Omega \nabla \xi_i \cdot \nabla \xi_j d\Omega = \int_\Omega f \xi_i d\Omega + \int_\Omega \nabla\varphi \cdot \nabla \xi_i d\Omega, \qquad i = 1, \ldots, n.$$

This can be rewritten in the matrix form $\mathbf{AC} = \mathbf{B}$, with matrix elements assigned as:

$$a_{ij} = -\int_{\Omega} \nabla\xi_i \cdot \nabla\xi_j d\Omega = -\int_{\Omega} \nabla\left(\omega\chi_i\right) \cdot \nabla\left(\omega\chi_j\right) d\Omega,$$

$$b_i = \int_{\Omega} f\xi_i d\Omega + \int_{\Omega} \nabla\varphi \cdot \nabla\xi_i d\Omega = \int_{\Omega} f\omega\chi_i d\Omega + \int_{\Omega} \nabla\varphi \cdot \nabla\left(\omega\chi_i\right) d\Omega.$$

Upon solution, numerical values of the coefficients $\{C_i\}_{i=1}^{n}$ are substituted into expression (28) that in turn is substituted into (27):

$$u = \omega \sum C_i\chi_i + \varphi. \tag{35}$$

The latter can be evaluated at any point inside the geometric domain Ω in order to visualize the temperature u.

Acknowledgments

This research is supported in part by the National Science Foundation grants DMI-0323514, DMI-9900171, DMI-0115133, and CCR-0112758, the National Institute of Standards (NIST) grant 60NANB2D0126. The mannequin head model is courtesy Tamal Dey, Geometric Modeling Group, The Ohio State University.

References

[1] N. Ahuja and J.-H. Chuang. Shape representation using a generalized potential field model. *IEEE Trans. on Pattern Analysis and Machine Intelligence*, 19(2):169–176, 1997.

[2] I. Babuska, U. Banerjee, and J.E. Osborn. Survey of Meshless and Generalized Finite Element Methods: A Unified Approach. *Acta Numerica*, 12:1–125, 2003.

[3] A. Biswas and V. Shapiro. Approximate distance fields with non-vanishing gradients. *Graphical Models*, 66(3):133–159, May 2004.

[4] J. Bloomenthal. *Introduction to Implicit Surfaces*. Morgan Kaufmann Publishers, 1997.

[5] Carl de Boor. *A Practical Guide to Splines*. Springer-Verlag, 1978.

[6] Sarah F. Frisken, Ronald N. Perry, Alyn P. Rockwood, and Thouis R. Jones. Adaptively sampled distance fields: A general representation of shape for computer graphics. In *Proceedings of the ACM SIGGRAPH Conference on Computer Graphics*, pages 249–254, 2000.

[7] K. Höllig. *Finite Element Methods with B-Splines*. Number 26 in Frontiers in Applied Mathematics. SIAM, 2003.

[8] Höllig K., Reif U., and Wipper J. Weighted extended b-spline approximation of dirichlet problems. *SIAM Journal on Numerical Analysis*, 39(2):442–462, 2001.

[9] L. V. Kantorovich and V. I. Krylov. *Approximate Methods of Higher Analysis*. Interscience Publishers, 1958.

[10] N. Kojekine, I. Hagiwara, and V. Savchenko. Software tools using csrbf's for processing scattered data. *Computers and Graphics*, 27(2), 2003.

[11] F. Leymarie and M. D. Levine. Fast raster scan distance propagation on the discrete rectangular lattice. *Computer Vision, Graphics, and Image Processing*, 55(1):84–94, January 1992.

[12] C. Lim, G. M. Turkiyyah, M. A. Ganter, and D. W. Storti. Implicit reconstruction of solids from cloud point sets. In *Proceedings of the Third Symposium on Solid Modeling and Applications*, pages 393–402. ACM Press, 1995.

[13] S.G. Mikhlin. *Variational methods in mathematical physics*. Oxford, New York, Pergamon Press, 1964.

[14] S. Muraki. Volumetric shape description of range data using "Blobby Model. *Proceedings of the ACM SIGGRAPH Conference on Computer Graphics*, 25(4):227–235, July 1991.

[15] Y. Ohtake, A. Belyaev, M. Alexa, G. Turk, and H.-P. Seidel. Multi-level partition of unity implicits. *ACM Transactions on Graphics (TOG)*, 22(3):463–470, 2003.

[16] Stanley Osher and Ronald Fedkiw. *Level Set Methods and Dynamic Implicit Surfaces*. Springer-Verlag, 2003.

[17] A. Pasko, V. Adzhiev, A. Sourin, and V. Savchenko. Function representation in geometric modeling:concepts, implementation and applications. *The Visual Computer*, 11(8):429–446, 1995.

[18] Alon Raviv and Gershon Elber. Three-dimensional freeform sculpting via zero sets of scalar trivariate functions. *Computer-Aided Design*, 32:513–526, 2000.

[19] W. Ritz. Über eine neue Methode zur Lösung gewisser Variationsprobleme der mathematischen Physik. *J. reine angew. Mathematik*, 135(1), 1908.

[20] V. L. Rvachev. *Theory of R-functions and Some Applications*. Naukova Dumka, 1982. In Russian.

[21] V. L. Rvachev and T. I. Sheiko. R-functions in boundary value problems in mechanics. *Applied Mechanics Reviews*, 48(4):151–188, 1996.

[22] V. L. Rvachev, T. I. Sheiko, V. Shapiro, and I. Tsukanov. On completeness of RFM solution structures. *Computational Mechanics*, 25:305–316, 2000.

[23] V. L. Rvachev, T. I. Sheiko, V. Shapiro, and I. Tsukanov. Transfinite interpolation over implicitly defined sets. *Computer Aided Geometric Design*, 18(4):195–220, 2001.

[24] V. L. Rvachev and N. S. Sinekop. *R-functions method in problems of the elasticity and plasticity theory*. Nauk. dumka, Kiev, 1990. In Russian.

[25] V.L. Rvachev and L.V. Kurpa. *R-functions in problems of the theory of plates*. Nauk. dumka, Kiev, 1987. In Russian.

[26] Vladimir V. Savchenko, Alexander A. Pasko, Oleg G. Okunev, and Tosiyasu L. Kunii. Function Representation of Solids Reconstructed from Scattered Surface Points and Contours. *Computer Graphics Forum*, 14(4):181–188, 1995.

[27] Benjamin Schmitt, Alexander Pasko, and Christophe Schlick. Constructive sculpting of heterogeneous volumetric objects using trivariate b-splines. *The Visual Computer*, 20(2):130–148, may 2004.

[28] V. Shapiro. Theory of R-functions and applications: A primer. Tech. Report TR91-1219, Computer Science Department, Cornell University, Ithaca, NY, 1991.

[29] V. Shapiro. Real functions for representation of rigid solids. *Computer-Aided Geometric Design*, 11(2):153–175, 1994.

[30] V. Shapiro. Well-formed set representations of solids. *International Journal on Computational Geometry and Applications*, 9(2):125–150, 1999.

[31] V. Shapiro. A convex deficiency tree algorithm for curved polygons. *International Journal of Computational Geometry and Applications*, 11(2):215–238, 2001.

[32] V. Shapiro and I. Tsukanov. Implicit functions with guaranteed differential properties. In *Fifth ACM Symposium on Solid Modeling and Applications*, pages 258–269, Ann Arbor, MI, 1999.

[33] V. Shapiro and I. Tsukanov. Meshfree simulation of deforming domains. *Computer-Aided Design*, 31(7):459–471, 1999.

[34] D. Shepard. A two-dimensional interpolation function for irregularly spaced data. In *Proceedings 23rd ACM National Conference*, pages 517–524, 1968.

[35] Gilbert Strang and George J. Fix. *An Analysis of the Finite Element Method*. Wellesley-Cambridge Press, 1988.

[36] I. Tsukanov and V. Shapiro. The architecture of SAGE – a meshfree system based on RFM. *Engineering with Computers*, 18(4):295–311, 2002.

[37] I. Tsukanov and V. Shapiro. Meshfree modeling and analysis of physical fields in heterogeneous media. *Advances in Computational Mathematics*, 2004. to appear.

[38] I. Tsukanov, V. Shapiro, and S. Zhang. A meshfree method for incompressible fluid dynamics problems. *International Journal for Numerical Methods in Engineering*, 58(1):127–158, 2003.

[39] G. Turk and J. O'Brien. Modeling with implicit surfaces that interpolate. *ACM Transactions on Graphics*, 21(4):855–873, October 1999.

[40] H. Zhao, S. Osher, and R. Fedkiw. Fast surface reconstruction and deformation using the level set method. *Proceedings of IEEE Workshop on Variational and Level Set Methods in Computer Vision, Vancouver*, July, 2001.